

MgB₂ Nonlinear Properties Investigated Under Localized High RF Magnetic Field Excitation

Tamin Tai*, B. G. Ghamsari, Steven M. Anlage, Center for Nanophysics and Advanced Materials, Physics Department, University of Maryland, College Park, MD 20742, USA.
C. G. Zhuang, X. X. Xi, Physics Department, Temple University, Philadelphia, PA 19122, USA

Abstract

In order to increase the accelerating gradient of Superconducting Radio Frequency (SRF) cavities, Magnesium Diboride (MgB₂) opens up hope because of its high transition temperature and potential for low surface resistance in the high RF field regime. However, due to the presence of the small superconducting gap in the π band, the nonlinear response of MgB₂ is potentially quite large compared to a single gap s-wave superconductor (SC) such as Nb. Understanding the mechanisms of nonlinearity coming from the two-band structure of MgB₂, as well as extrinsic sources, is an urgent requirement. A localized and strong RF magnetic field, created by a magnetic write head, is integrated into our nonlinear-Meissner-effect scanning microwave microscope [1]. MgB₂ films with thickness 50 nm, fabricated by a hybrid physical-chemical vapor deposition technique on dielectric substrates, are measured at a fixed location and show a strongly temperature-dependent third harmonic response. We propose that at least two mechanisms are responsible for this nonlinear response, one of which involves vortex nucleation and penetration into the film.

INTRODUCTION

The discovery of superconductivity in MgB₂ in January 2001 [2] ignited enthusiasm and interest in exploring its material properties. Several remarkable features, for example a high transition temperature ($T_c \sim 40$ K), a high critical field, and a low RF surface resistance below T_c , shows great potential in several applications such as superconducting wires and magnets. The success of making high quality epitaxial MgB₂ thin films provides another promising application as an alternative material coating on superconducting radio frequency (SRF) cavities [3]. Over the past decade, the improvement of accelerating gradient in Niobium (Nb) SRF cavities has almost reached the BCS limit, 57 MeV/m [4]. In order to go further, new high T_c materials with low RF resistance are required for interior coating of bulk Nb cavities. High quality MgB₂ thin films may satisfy the demands for SRF coating materials because these high quality films can avoid the weak link nonlinearity between grains, and lead to the possibility of making high-Q cavities [5].

However, there still exist mechanisms that produce non-ideal behavior at low temperatures under high RF magnetic fields, such as vortex nucleation and motion in the film [6]. In addition, due to the π band and σ band,

the intrinsic nonlinear Meissner effect of MgB₂ is large compared to other single-gap s-wave superconductors [7]. Therefore the study of MgB₂ microwave nonlinear response in the high frequency region (usually several GHz in SRF applications) can reveal the dissipative and nondissipative nonlinear mechanisms and allow application of these high quality MgB₂ films as cavity coatings.

In our experiment the localized harmonic response of superconductors is excited by a magnetic write head probe extracted from a commercial magnetic hard drive [1]. Based on the gap geometry of the magnetic write head probe, sub micron resolution is expected. We present our observation of at least two measurable nonlinear mechanisms involved in high quality MgB₂ films below T_c . These films were grown on sapphire substrates by hybrid physical-chemical vapor deposition technique (HPCVD). A detailed description of the growth technique has been reported before [8]. Finally, experimental nonlinearity data will be interpreted as a combination of intrinsic nonlinear response [9] and vortex nonlinearity [6].

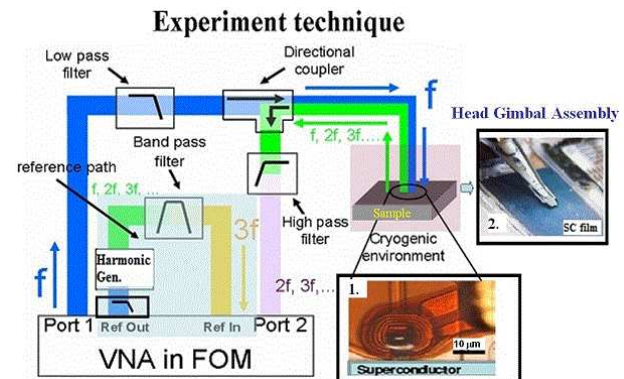


Figure 1: Set up of phase-sensitive measurement in nonlinear microwave microscopy. The frequency offset mode (FOM) of a vector network analyzer (VNA :model PNA-X N5242A) is used in this measurement. Inset 1. is a schematic picture of the probe above the sample and inset 2 shows the magnetic write head probe assembly on top of a superconducting thin film.

EXPERIMENTAL SETUP

The experimental setup for amplitude and phase measurements of the superconductor harmonic response is shown in Fig. 1. An excited wave (fundamental sig-

*tamin@umd.edu

nal) at frequency f comes from the vector network analyzer (VNA) and is low-pass filtered to eliminate higher harmonics of the source signal. This fundamental tone is sent to the magnetic write head probe to generate a localized RF magnetic field on the superconductor sample. Two insets in Fig. 1 shows close-up views of our magnetic write head probe on superconducting samples. Due to the intense nature of this field, the superconductor responds by generating currents at both the fundamental frequency and at harmonics of this frequency. The generated harmonic signal is high-pass filtered to remove the fundamental signal V_f and an un-ratioed measurement of V_{3f} is performed on port 2 of the VNA. In order to get a phase-sensitive measurement of the 3^{rd} harmonic signal coming from the superconducting sample, a harmonic generation circuit is connected to provide a reference 3^{rd} harmonic signal, and the relative phase difference between the main circuit and reference circuit is measured. Further detail about this phase-sensitive measurement technique can be found in Ref. [10]. In this way we measure the complex third harmonic voltage of $V_{3f}^{sample}(T)$ or the corresponding scalar power $P_{3f}^{sample}(T)$. The lowest noise floor in our VNA is -145 dBm for the un-ratioed power measurement. A ratioed measurement of the complex $V_{3f}^{sample}(T)/V_{3f}^{ref}$ is also performed at the same time. In this paper we only discuss the un-ratioed measurements of $P_{3f}^{sample}(T)$ and qualitatively discuss the mechanisms of third harmonic response of the MgB_2 film.

THIRD ORDER NONLINEAR MEASUREMENT RESULTS

The measurement of the 3^{rd} order harmonic power (P_{3f}) is performed near the center of the epitaxial MgB_2 film of thickness 50 nm. The T_c of this sample is 36 K as measured by the four point resistance method. Figure 2 shows the temperature dependent $P_{3f}(T)$ curves at the excited frequency 5.33 GHz and excited power +14 dBm. Above 40 K a very small signal begins to arise above the noise floor of the network analyzer. This P_{3f} is from the magnetic write head probe itself. We have measured the P_{3f} of the magnetic probe on the surface of a bare sapphire substrate and in general this probe nonlinearity is negligible at excited powers under 14 dBm. Although excited powers above +14 dBm excites stronger nonlinearity from the probe, this nonlinearity is almost temperature independent in the Helium cooling temperature range. Therefore probe nonlinearity can be treated as a constant background signal above the noise floor of the spectrum analyzer. The mechanism of probe nonlinearity is the hysteretic behavior of the yoke material [11] and has been discussed previously [1].

From Fig. 2, a clear $P_{3f}(T)$ peak centered at 35 K shows up above the noise floor. This peak arises from the intrinsic nonlinear Meissner Effect (NLME) at T_c due to the enhanced sensitivity of superconducting properties as the superfluid density decreases to near-zero levels. This peak at T_c is also phenomenologically predicted by Ginzburg-

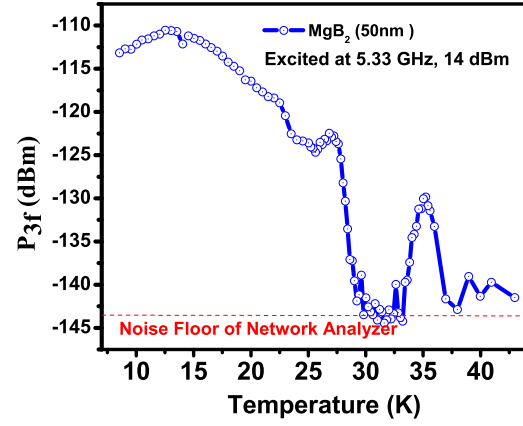


Figure 2: Temperature dependence of 3rd harmonic power P_{3f} from a 50 nm thick MgB_2 measured with an excited frequency of 5.33 GHz.

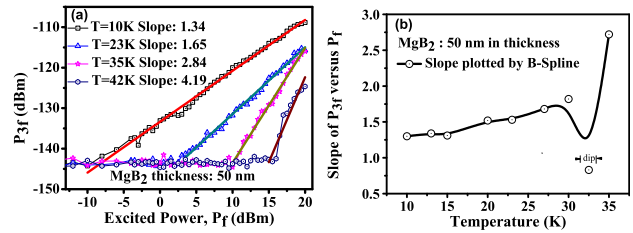


Figure 3: (a) Power dependence of P_{3f} on P_f for the 50 nm thick MgB_2 film. (b) Fitted slope at selected temperatures for the film. The marked dip may describe a vortex-free region and its small slope is likely due to the probe nonlinearity.

Landau theory, and is discussed further below.

We also note the onset of a low temperature nonlinearity below 27 K, which implies that another temperature dependent nonlinear mechanism is active. It may be that the applied RF field from the probe is strong enough to penetrate into the superconductor and create deep flux penetration or even Abrikosov vortices in a localized area. This new nonlinear mechanism dominates the overall measured nonlinearity in the low temperature region. Further qualitative discussion of the low temperature nonlinearity from a possible Abrikosov vortex critical state will be addressed in detail below.

In addition, in the temperature regime of $29K \sim 33K$, there is a minimum P_{3f} signal, which implies no strong nonlinearity mechanisms in this temperature range. The supercurrent of a vortex circulates around the normal core with an approximate size of the magnetic penetration depth $\lambda(T)$. Therefore once $\lambda(T)$ is bigger than the film thickness (50 nm in this case) above a certain temperature, vortex penetration due to parallel magnetic field will be suppressed [12]. This regime would be very suitable to fabricate a low nonlinearity superconducting response in a multi-layer superconductor / insulator structure [13].

Measurements of the dependence of P_{3f} on P_f are

shown in Fig. 3 (a) for the 50 nm thick MgB₂ film at some selected temperatures. In the normal state of MgB₂, the measured nonlinearity comes from the probe itself and shows a slope steeper than 3 at high excited power above +15 dBm. In the intrinsic nonlinear Meissner regime, the slope is 2.84, very close to 3 as predicted for the intrinsic NLME [14]. Based in part on this evidence, we believe that in the high temperature region close to T_c , the P_{3f} comes from the intrinsic NLME. In the low temperature regime, the slopes of P_{3f} vs. P_f are around 1.5. This value is similar to that predicted by many phenomenological models (between 1 ~ 2) in an Abrikosov vortex critical state [15] [16]. It should be noted that the low temperature nonlinearity can be easily excited at low power. Figure 3 (b) show the P_{3f} - P_f slope evolution from a flux/vortex dominated nonlinear regime at low temperature to a NLME regime around T_c for this MgB₂ film.

INTRINSIC NLME OF MGB₂

The intrinsic nonlinearity comes from the backflow of excited quasiparticles in a current-carrying superconductor, which results in an effective decrease of the superfluid density. Therefore, a two band quasiparticle backflow calculation should be applied to the MgB₂ intrinsic nonlinearity. Based on the work of Dahm and Scalapino[9], the temperature and induced current density dependent superfluid density $n_s(T, J)$ can be written as

$$\frac{n_s(T, J)}{n_s(T, 0)} = 1 - \left(\frac{J}{J_{NL}}\right)^2; J_{NL} = \frac{J_{c,\pi}}{\sqrt{b_\pi(T) + b_\sigma(T) \frac{J_{c,\pi}^2}{J_{c,\sigma}^2}}} \quad (1)$$

where b_σ and b_π are the temperature dependent nonlinear coefficients for the σ band and π band, respectively, and their values are defined in reference [9]. $J_{c,\sigma} = 4.87 \times 10^8 A/cm^2$ and $J_{c,\pi} = 3.32 \times 10^8 A/cm^2$ are the pair-breaking current densities for the two bands. For a 50 nm thick MgB₂ thin film, the generated third harmonic power $P_{3f}(T)$ is estimated by substituting J_{NL} into the following equation [14]

$$P_{3f}(T) = \frac{\omega^2 \mu_0^2 \lambda^4(T) \Gamma^2}{32 Z_0 d^6 J_{NL}^4(T)} \quad (2)$$

where ω is the angular frequency of the incident wave, d is the film thickness, $\lambda(T)$ is the temperature dependent magnetic penetration depth, Z_0 is the characteristic impedance of the transmission line in the microscope, and Γ is geometry factor which is estimated to be $10^5 A^3/m^2$ for the magnetic write head field distribution under a 100 mW excited power. The solid red line in Fig. 4 shows the $P_{3f}(T)$ simulated results of Eqs. (1) and (2) for the 50 nm thick film at a 5.33 GHz excited frequency. This intrinsic NLME response has measurable values above the noise floor only in the high temperature region near T_c . The experimental data of the MgB₂ film under a +18 dBm, 5.33 GHz microwave excitation is shown in the blue dots. Therefore, at

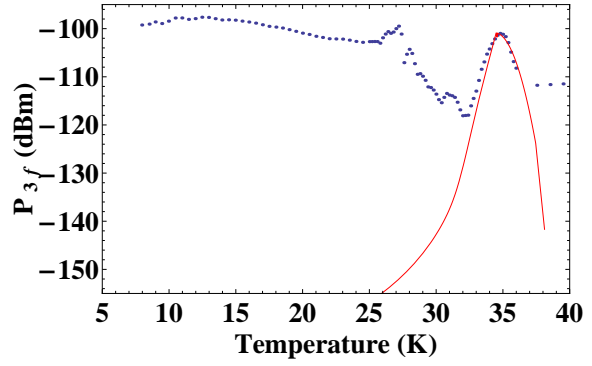


Figure 4: Solid red line is the simulated result of the intrinsic NLME of MgB₂ with thickness 50 nm under the assumption that the magnetic probe provides a field described by a geometry factor $\Gamma = 8.3 \times 10^5 A^3/m^2$. Other parameters used in this calculation include $\lambda(0K)=100 nm$, $\lambda_{cutoff}=800 nm$, $J_{cutoff} = 4.2 \times 10^{11} A/m^2$ and $T_c=34.6 K$ with a standard deviation of Gaussian spread of $\delta T_c=1.3 K$. The blue dots are the data from the experiment.

lower temperatures the nonlinear mechanism must be of a different nature.

NONLINEARITY IN ABRIKOSOV VORTEX CRITICAL STATE

Nonlinearity From Moving Vortices

Vortex nucleation and penetration into the film induces a dynamic instability and generates harmonic response. The equation of motion of a vortex in a semi-infinite superconductor driven by a harmonic magnetic field is given by [6]

$$\eta \dot{x} = \frac{\Phi_0 B_0}{\mu_0 \lambda(T)} e^{i\omega t} e^{-x/\lambda(T)} - \frac{\Phi_0^2}{2\pi \mu_0 \lambda^3(T)} K_1\left(\frac{2\pi x}{\lambda(T)}\right) \quad (3)$$

where x is the coordinate of the vortex position with respect to the surface ($x=0$), η is the Bardeen-Stephen vortex viscosity, Φ_0 is the flux quantum, ω is the angular frequency of the incident wave, μ_0 is the permeability of vacuum, B_0 is the magnitude of RF magnetic field on the SC surface and $K_1(x)$ is the modified Bessel function. The first term on the right hand side is the Lorentz force per unit length on the vortex due to the screening currents created by the driving field. The second term on the right is the force per unit length exerted by the image vortex that arises from the SC/vacuum surface. This equation assumes a bulk superconductor.

The solution for the trajectory of this single vortex is shown in Fig. 5 as a function of time in the lower solid blue curve. The applied RF field $B(t)$ is also included in the figure to illustrate the relation of the vortex position and the applied field with time. The time for the first vortex entry can be determined as [6],

$$t_0 = \frac{\arcsin\left(\frac{B_w}{B_0}\right)}{\omega} \quad (4)$$

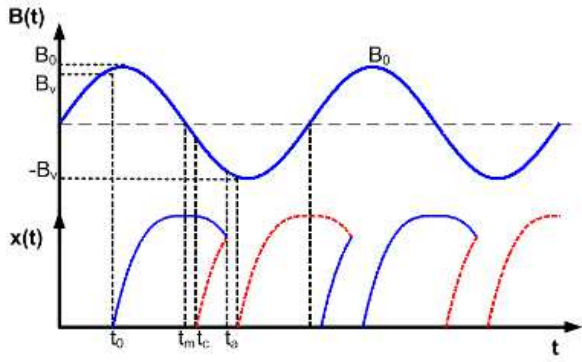


Figure 5: A calculation of vortex position $x(t)$ with the applied RF field $B(t)$ over several RF cycles. Here t_0 indicates the time of vortex entry, t_m is the time when the vortex reaches its maximum distance into the film, t_c is the antivortex nucleation time, and t_a is the vortex / anti-vortex collision time.

where B_v is the penetration field of a vortex (assuming $B_v < B_0$). A vortex will start to nucleate and enter into the film when $B(t)$ exceeds the Bean-Livingston barrier [17]. This vortex also creates a supercurrent circulating around the core and distorts the Meissner screening current near the surface. During the reverse part of the RF cycle, the Meissner screening current is enhanced so that at time t_c an anti-vortex will penetrate into the superconductor as shown by the dashed red line. This second vortex will annihilate with the first vortex at time t_a . This procedure of vortex-antivortex entry and annihilation continues and will generate a third harmonic signal.

For further quantitative modeling, the following two cases should be taken into consideration:

(1) Finite thickness of the film.

The vortex equation of motion given above is only suitable for bulk materials and assumes that a uniform magnetic field is applied parallel to the SC surface. In the finite thickness case, an infinite number of image vortices are required to satisfy the boundary conditions. However we can make an approximation that only two image vortices are required. Therefore the equation of motion of the vortex is modified to,

$$\eta \dot{x} = \frac{\Phi_0 B_0}{\mu_0 \lambda} e^{i\omega t} e^{-x/\lambda} - \frac{\Phi_0^2}{2\pi\mu_0\lambda^3} \left[K_1\left(\frac{2\pi x}{\lambda}\right) - K_1\left(\frac{2\pi(d-x)}{\lambda}\right) \right] \quad (5)$$

where d is the thickness of the film. This modification for a second image force will help improve the quantitative modeling.

(2) surface roughness of the film

In the Bean-Livingston model the superconducting surface is assumed to be a perfect plane [17]. When the surface has roughness with characteristic length $\geq \xi$ (coherence length), a geometry effect should be taken

into consideration [18]. Generally, for a sharper corner, the Meissner screening current density will be enhanced and the penetration field of the first vortex entry (B_v) will decrease. For example, at a corner with a 90° angle, an enhancement of the screening current is roughly estimated to be a factor of 4 [18]. This means a vortex will penetrate at sharp points or cusps easily and reduce the vortex nucleation time during the RF cycle. Therefore, nonlinear harmonic response will be increased compared to the case of a perfect plane. Hence for a given excitation level, the harmonic response will depend on the surface topography, and an image showing this contrast can be built up by raster scanning the magnetic probe.

Nonlinearity From Switching Between the Meissner State and the Vortex Critical State

In addition to vortex and antivortex nucleation and motion, another possibility to generate a P_{3f} in the Abrikosov vortex critical state is the switching between this state and the nonlinear Meissner state. While the peak value of the applied RF magnetic field is higher than the surface penetration field of the superconductor, the material will switch into the critical vortex state from the Meissner state. This process of switching between states implies another source of nonlinear harmonic response.

Fig. 6 (a) shows a schematic illustration of our experiment in which the RF magnetic field from the magnetic write head probe interacts with the superconductor underneath the probe. One can model the flux distribution with an equivalent magnetic circuit as shown in Fig.6 (b). The inductively coupled driving line provides a magnetomotive force (V_m) to the yoke with a reluctance R_y . A magnetic flux Φ is channeled down along the yoke to the gap. There the flux can divide into two branches: one directly goes through the gap with a reluctance R_g and the other shunts into the superconductor with a reluctance R_{sc} . The reluctance of superconductor R_{sc} is a time-variable reluctance. It is a combination of the reluctance R_s from the nonlinear Meissner state and the reluctance R_v from the vortex critical state. While the applied field $B(t)$ is smaller than the penetration field B_v , the reluctance will remain at the value of R_s . Once $B(t) \geq B_v$, an additional reluctance channel R_v is created. Whether the vortex enters as a semi-loop (as assumed above), or as a vortex-antivortex pair, remains to be evaluated.

Because a magnetic circuit is analogous to an electric circuit, we can compute R_v and R_s with node-voltage analysis. Assume that the flux going through R_g and R_{sc} is ϕ_g and ϕ_{sc} , respectively. In the nonlinear Meissner state, we obtain

$$\phi_g = B_0 A_{gap} = B_0(w * g) \quad ; \quad \phi_{sc} = B_0(w * \lambda) \quad (6)$$

where A_{gap} is the cross-sectional area of the gap, w and g are the width and the thickness of the gap, respectively (see Fig. 6 (a)), and λ is temperature dependent penetration

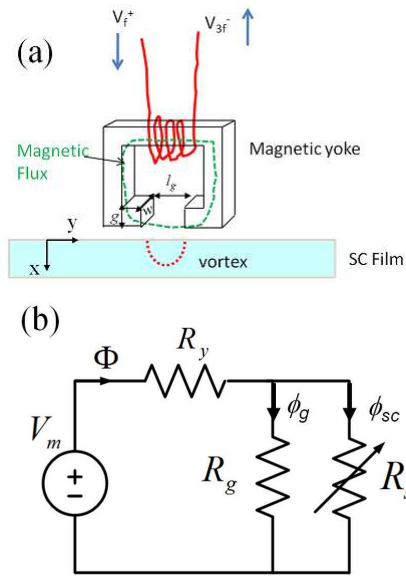


Figure 6: (a) Schematic illustration of the magnetic flux coming from the yoke to the superconductor where w , g and l_g represent the width, the thickness, and the length of the gap, respectively. The length l_g is on the order of 200 nm for our write head probe. (b) An equivalent magnetic circuit for the magnetic flux transport from the yoke to the superconductor. Note $R_{sc}=R_s+R_v$ is a time variable reluctance..

depth. Applying the node-voltage law, we have $\phi_g R_g = \phi_{sc} R_s$. Finally, the reluctance of the nonlinear Meissner state is given by

$$R_s = \frac{g}{\lambda} R_g \quad R_g = \frac{l_g}{\mu_0 A_{gap}} \quad (7)$$

where l_g is the length of the gap (see Fig. 6 (a)) and μ_0 is the permeability of vacuum. On the other hand, in the vortex critical state, we have the magnetomotive force as

$$\phi_0 R_v = \int_{gap} H_0 dy = \frac{B_0 l_g}{\mu_0} \quad \phi_0 = B_0 \lambda^2 \quad (8)$$

where ϕ_0 is the flux quantum and the latter equation assumes that the vortex carries one unit of magnetic flux, which may not always be the case. Hence the reluctance of the vortex critical state is $R_v = \frac{l_g}{\mu_0 \lambda^2}$. In addition to the nonlinearity of the penetration depth with RF field, we believe the transient between R_v and R_s will also induce a third harmonic response.

CONCLUSIONS

A strongly temperature-dependent third harmonic response is found in high quality MgB₂ films. In addition to the intrinsic nonlinearity, the nonlinearity coming from the Abrikosov critical state may also be involved. From the dependence of P_{3f} on P_f , the nonlinearity mechanism

changes from an intrinsic nonlinear Meissner effect to a possible vortex critical state dominated nonlinearity upon cooling the high quality epitaxial MgB₂ film. The mechanics of nonlinearity in the Abrikosov vortex critical state can be qualitatively interpreted by two models - first: annihilation of moving vortex & antivortex pairs and second: state switching between a Meissner state and a vortex critical state.

ACKNOWLEDGEMENT

This work is supported by the US Department of Energy/ High Energy Physics through grant # DESC0004950, and also by the ONR AppEl, Task D10, (Award No. N000140911190), and CNAM. The work at Temple University is supported by DOE under grant No. de-sc0004410.

REFERENCES

- [1] T. M. Tai, X. X. Xi, C. G. Zhuang, D. I. Mircea, S. M. Anlage, "Nonlinear Near-Field Microwave Microscope for RF Defect Localization in Superconductors," IEEE Trans. Appl. Supercond. **21**, 2615 (2011).
- [2] J. Nagamatsu, Norimasa Nakagawa, Takahiro Muranaka, Yuji Zenitani, Jun Akimitsu, "Superconductivity at 39K in Magnesium Diboride," Nature **410**, 63 (2001).
- [3] X. X. Xi, "Topical Review - MgB₂ thin films", Supercond. Sci. Technol. **22**, 043011 (2009).
- [4] TeV-Energy Superconducting Linear Accelerator, TESLA Technical Design Report, Hamburg: Deutsches Elektronen-Synchrotron DESY, 2001, http://flash.desy.de/tesla/tesla_documentation.
- [5] T. Tajima, A. Canabal, Y. Zhao, A. Romanenko, B. H. Moeckly, C. D. Nantista, S. Tantawi, L. Phillips, Y. Iwashita and I. E. Campisi, "MgB₂ for Application to RF Cavities for Accelerators", IEEE Trans. Appl. Supercond. **17**, 1330 (2007).
- [6] A. Gurevich, G. Ciovati, "Dynamics of Vortex Penetration," Phys. Rev. B **77**, 104501 (2008).
- [7] G. Cifariello, M. Aurino, E. D. Gennaro, G. Lamura, A. Andreone, P. Orgiani, X. X. Xi, "Intrinsic Nonlinearity Probed by Intermodulation Distortion Microwave Measurements on High Quality MgB₂ Thin Films," Appl. Phys. Lett. **88**, 142510 (2006).
- [8] X. Zeng, A. V. Pogrebnikov, A. Kotcharov, J. E. Jones, X. X. Xi, E. M. Lyszczek, J. M. Redwing, S. Y. Xu, J. Lettieri, D. G. Schlom, W. Tian, X. Q. Pan, Z. K. Liu, "In Situ Epitaxial MgB₂ Thin Films for Superconducting Electronics," Nature Materials **1**, 35 (2002).
- [9] T. Dahm, D. J. Scalapino, "Nonlinear Microwave Response of MgB₂," Appl. Phys. Lett. **85**, 4436 (2004).
- [10] D. I. Mircea, H. Xu, S. M. Anlage, "Phase-sensitive Harmonic Measurements of Microwave Nonlinearities in Cuprate Thin Films" Phys. Rev. B **80**, 144505 (2009).
- [11] Charles P. Bean, "Magnetization of High-Field Superconductors," Rev. Mod. Phys. **36**, 31 (1964).

- [12] E. Guyon, F. Meunier, R. S. Thompson, "Thickness Dependence of κ_2 , and Related Problems for Superconducting Alloy Films in Strong Fields," Phys. Rev. **156**, 452 (1967).
- [13] A. Gurevic, "Enhancement of RF Breakdown Field of Superconductors by Multilayer Coating," Appl. Phys. Lett. **88**, 012511 (2006).
- [14] S. C. Lee, M. Sullivan, G. R. Ruchti, and S. M. Anlage, B.S. Palmer, B. Maiorov, E. Osquiguil, "Doping-dependent Non-linear Meissner Effect and Spontaneous Currents in High-Tc Superconductors," Phys. Rev. B **71**, 014507, (2005).
- [15] D. E. Oates, S. H. Park, M. A. Hein, P. J. Hirst, and R. G. Humphreys, "Intermodulation Distortion and Third-harmonic Generation in YBCO Films of Varying Oxygen Content," IEEE Trans. Appl. Supercond. **13**, 311 (2003).
- [16] J. Mateu, C. Collado, O. Menendez, and J. M. O'Callaghan, "A General Approach for the Calculation of Intermodulation Distortion in Cavities with Superconducting Endplates," Appl. Phys. Lett. **82**, 97 (2003).
- [17] C. P. Bean, J. D. Livingston, "Surface Barrier in Type-II Superconductors," Phys. Rev. Lett. **12**, 14 (1964).
- [18] Ernst Helmut Brandt, "Electrodynamics of Superconductors Exposed to High Frequency Fields", arXiv:1008.2231.